Chinese Chemical Letters 36 (2025) 110762

Contents lists available at ScienceDirect

Chinese Chemical Letters

journal homepage: www.elsevier.com/locate/cclet

Thermally robust bis(imino)pyridyl iron catalysts for ethylene polymerization: Synergy effects of weak π-π interaction, steric bulk, and electronic tuning

Heng Gao, Zhaocong Cheng, Guangshui Tu, Zonglin Qiu, Xieyi Xiao, Haotian Zhou, Handou Zheng*, Haiyang Gao*

School of Materials Science and Engineering, PCFM Lab, GD HPPC Lab, DSAPM Lab, Sun Yat-sen University, Guangzhou 510275, China

ARTICLE INFO

Article history:
Received 11 October 2024
Revised 9 December 2024
Accepted 12 December 2024
Available online 13 December 2024

Keywords:
Bis(imino)pyridyl iron
π-π Interaction
Steric effect
Electronic effect
Ethylene polymerization

ABSTRACT

A series of "half-sandwich" bis(imino)pyridyl iron complexes with a substituted 8-(*p*-X-phenyl)naphthylamine (X = OMe, Me, CF_3) was designed and synthesized by combining weak π-π interaction with steric and electronic tunings. The weak noncovalent π-π interaction as well as the steric and electronic effects of bis(imino)pyridyl iron complexes were identified by experimental analyses and calculations. The roles of weak π-π interaction, steric bulk, and electronic tuning on the ethylene polymerization performance of bis(imino)pyridyl iron catalysts were studied in detail. The combination of π-π interaction with steric and electronic tunings can access to thermally stable bis(imino)pyridyl iron at 130 °C.

© 2025 Published by Elsevier B.V. on behalf of Chinese Chemical Society and Institute of Materia Medica, Chinese Academy of Medical Sciences.

Since the seminal work on bis(imino)pyridyl iron and cobalt catalysts by Brookhart and Gibson, bis(imino)pyridyl iron olefin polymerization catalysts have attracted tremendous interest due to their non-toxicity, high metal abundance, and high activity [1–6]. As a kind of unique late transition metal catalysts of ethylene polymerization or oligomerization, bis(imino)pyridyl iron catalysts produced fully linear products without branches. Therefore, bis(imino)pyridyl iron catalysts are promising candidates for delivering high-density polyethylene (HDPE), polyethylene (PE) wax, and linear α-olefins [7–9]. However, late transition metal catalysts often show poor thermal stability and temperature tolerance, which restricts their industrial application [10–12]. A tremendous number of efforts have been contributed to developing thermally robust bis(imino)pyridyl iron catalysts [13–18].

In general, two strategies including steric and electronic tunings are widely employed to access to thermally stable bis(imino)pyridyl iron catalysts, especially bulky *N*-aryl substituents based on the steric demand proposed by Brookhart (Figs. 1A and B) [19,20]. Despite great developments in bis(imino)pyridyl iron catalysts, the steric and electronic modification strategies often exhibit a conflicting "see-saw" effect. Sterically bulky *N*-aryl substituents of bis(imino)pyridyl iron catalysts often lead to a significant decrease in catalytic activity because of their inhibition of the coordination and insertion of ethylene monomer. For example, bis(imino)pyridyl iron catalysts with bulky 2,6-dibenzhydrylaniline moieties (Fig. 1C) reported by Sun and Long are inactive for ethylene polymerization [21,22]. Pentiptycenyl-substituted bis(imino)pyridyl iron catalysts (Fig. 1D) reported by Jian also exhibit low activity to produce unexpected low-molecular-weight product (M_n < 2500 g/mol) [23]. Alternatively, the asymmetrical approach including 2,6-asymmetrically substituted aniline (Fig. 1E) and two different anilines (Fig. 1F) is further utilized to balance the steric bulk to improve the polymerization properties of bis(imino)pyridyl iron catalysts [24–26].

In addition to well-known steric and electronic tunings, weak noncovalent interactions are another effective tool in controlling olefin polymerization catalysis [27,28]. Unlike steric and electronic modifications involving covalent bonding interactions, noncovalent interactions not only affect the coordination geometry of catalyst but also impact monomer reactivity, selectivity, and growing chain structure during olefin polymerization [29,30]. The weak noncovalent interactions such as hydrogen bonding [31,32], π-π interactions [33–35], metal-aryl π-interactions [36,37] and electrostatic metal-X interactions (X = heteroatoms) [38,39] have been widely applied in modulating transition metal-catalyzed polymerization of olefins (M = Ti, Zr, Ni, Pd). However, the application of weak noncovalent interactions in the design of bis(imino)pyridyl iron catalysts is rarely reported to the best of our knowledge before.

* Corresponding authors.
E-mail addresses: zhenghdou@mail.sysu.edu.cn (H. Zheng), gaohy@mail.sysu.edu.cn (H. Gao).

https://doi.org/10.1016/j.cclet.2024.110762
1001-8417/© 2025 Published by Elsevier B.V. on behalf of Chinese Chemical Society and Institute of Materia Medica, Chinese Academy of Medical Sciences.

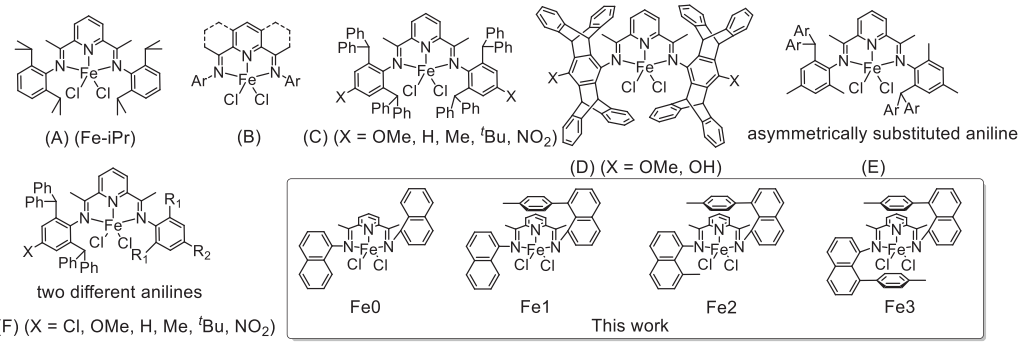

Fig. 1. Bis(imino)pyridyl iron complexes bearing various *N*-aryl substituents and four bis(imino)pyridyl iron complexes in this work.

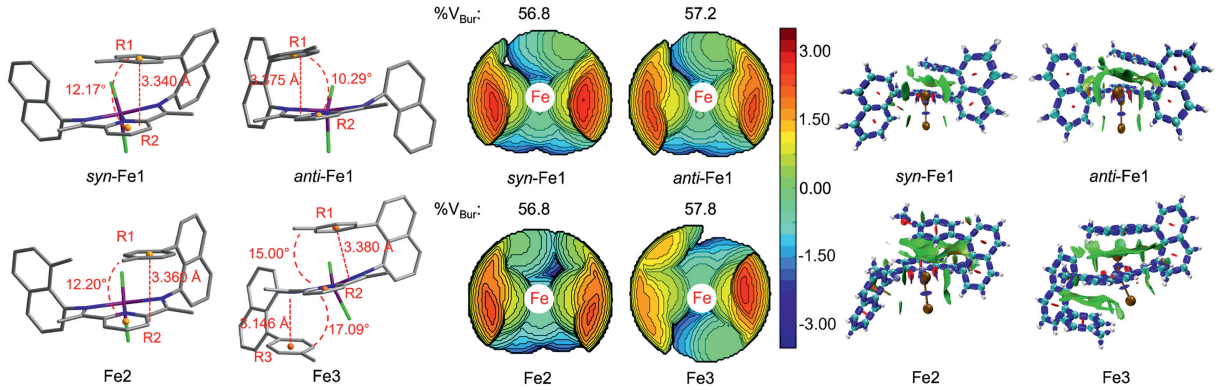

Fig. 2. Molecular structures, topographic steric map, and π-π interaction regions of bis(imino)pyridyl iron complexes.

our recent work involving weak π-π interactions in "sandwich" bis(imino)pyridyl iron catalysts [40].

In this paper, we intended to develop thermally robust bis(imino)pyridyl iron catalysts by cooperatively combining weak noncovalent interactions with steric and electronic tunings. A series of "half-sandwich" bis(imino)pyridyl iron complexes with a substituted 8-(*p*-X-phenyl)naphthylamine (X = OMe, Me, CF_3) were designed and synthesized. The roles of the steric and electronic tunings as well as π-π interactions are disclosed and they cooperatively operate ethylene polymerization to access to thermally robust bis(imino)pyridyl iron catalysts.

Based on decreasing steric bulk, "half-sandwich" bis(imino)pyridyl iron complexes with a capping aryl substituent were firstly designed. Two bis(imino)pyridyl ligands (L1, L2) were synthesized by a two-step condensation reaction of 2,6-diacetylpyridine with the corresponding substituted naphthylamine in high yield (Scheme S1 in Supporting information). All the ligands were fully characterized by ^{1}H and ^{13}C NMR spectroscopy as well as elemental analysis. New iron complexes (Fe1, Fe2) were readily synthesized by the complexation reaction of the corresponding bis(imino)pyridyl ligands with $FeCl_2$ in THF solvent. The purity and identity of iron complexes were confirmed by elemental analysis, IR, and X-ray diffraction analysis. For example, the characteristic absorption bands of the imine group (C=N) have obvious bathochromic-shift ($\sim$20 cm^{-1}) after ligation reaction from ligands to complexes (see ligand and complex characterization in Supporting information). To clearly demonstrate the effect of the capping aryl groups, bis(imino)pyridyl iron complex Fe0 with two naphthyl groups and "sandwich" bis(imino)pyridyl iron complex Fe3 with two capping 4-methylphenyl substituents were synthesized and used as comparisons (Scheme S1) [40,41].

Single crystals of two "half-sandwich" bis(imino)pyridyl iron complexes suitable for X-ray diffraction analysis were obtained through the slow diffusion of complex solution in CH_2Cl_2/hexane mixture solvent. As shown in Fig. 2, the capping aryl substituent is positioned above the chelate ring, and both iron complexes with a capping aryl group display a "half-sandwich" structure. In principle, there are *syn*- and *anti*-diastereomers of "half-sandwich" iron complexes because the two naphthyl rings are oriented on the same or contrary side of the chelate ring [42]. Fortunately, single crystals of *syn*- and *anti*-diastereomers of iron complex Fe1 were obtained, indicating that *syn*- and *anti*-diastereomers were present together and/or may transform each other in solution.

The capping aryl substituent provides steric hindrance around the iron center, which is calculated by the space-filling capabilities of the metal center. The calculated buried volumes (%V_{Bur}) of *syn*- and *anti*-Fe1, Fe2, and Fe3 are 56.8, 57.2, 56.8, and 57.8, respectively (Fig. 2) [43]. Clearly, the "sandwich" bis(imino)pyridyl iron complex Fe3 shows bulkier steric hindrance than its "half-sandwich" analogues. It is found that *syn*-Fe2 has the same %V_{Bur} value as *syn*-Fe1, although a methyl is installed on *syn*-Fe2. This result indicates that the capping 4-methylphenyl substituent dominates the steric hindrance. It is noteworthy that *syn*- and *anti*-Fe1 have nearly the same %V_{Bur} (relative error: 0.7%), which is also attributed to dominant steric bulk of the capping aryl substituent. It is anticipated that *syn*- and *anti*-diastereomers of Fe1 should have nearly the same ethylene polymerization behavior due to same steric effect. Therefore, we do not distinguish *syn*- and *anti*-diastereomers of iron complexes in the following discussion.

Like our previously reported "sandwich" bis(imino)pyridyl iron complexes [40], "half-sandwich" bis(imino)pyridyl iron complexes also exhibit an intramolecular π-π interaction between the capping aryl substituent and the pyridyl ring with offset face-to-face pattern. Crystal parameters in Table S1 (Supporting information) reveal that dihedral angles between the capping aryl group and the pyridyl ring are below 20° and the centroid-centroid distances of the two aromatic rings are within 3.5 Å, strongly supporting the presence of intramolecular π-π interaction in "half-sandwich"

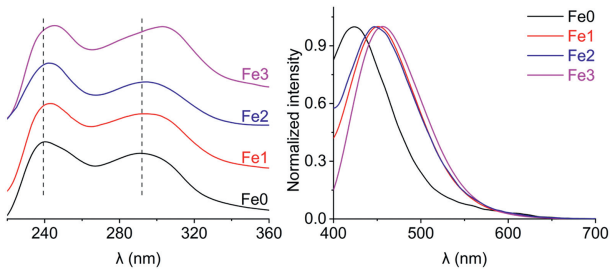

Fig. 3. UV–vis absorptions (left) and photoluminescence (PL) spectra (right) of iron complexes in CH_2Cl_2 solution.

bis(imino)pyridyl iron complexes. Besides, the π-π interaction regions (green regions) in iron complexes were directly and graphically shown in Fig. 2 through the space function interaction region indicator (IRI) [44].

In addition to X-ray single crystal structures, the existence of the intramolecular π-π interaction of iron complexes in solution were also spectroscopically proven [40]. As shown in Fig. 3, the UV–vis spectra of iron complexes in CH_2Cl_2 solvent reveal that iron complexes exhibit two absorption peaks at 240 and ~290 nm. Compared to iron complex Fe0 without the capping aryl substituents, the three iron complexes with capping aryl substituents exhibit a bathochromic-shifted absorption at ~300 nm (Fe3 > Fe2 ≈ Fe1 > Fe0), which can be ascribed to the π-π interactions in the iron complexes. Meanwhile, the associated photoluminescence (PL) spectra of these iron complexes also have obvious bathochromic-shift phenomenon. The iron complex Fe0 without the capping aryl substituent exhibits an emission peak centered at 423 nm irradiated by 365 nm excitation, while the other three iron complexes display bathochromic-shifted emission profiles (Fe3 > Fe1 ≈ Fe2 > Fe0) (Fig. 3). In general, installation of a capping aryl on "half-sandwich" bis(imino)pyridyl iron complexes not only can provide appropriately bulky steric hindrance but also can keep the π-π interaction.

In addition to steric hindrance, electronic tuning is also considered for the design of bis(imino)pyridyl iron catalysts. Two "half-sandwich" bis(imino)pyridyl iron complexes with substituted 8-(*p*-X-phenyl)naphthylamine (X = OMe, CF_3) were further prepared according to the same synthetic routine shown in Scheme S1. Single crystal of Fe4 was obtained, while Fe5 was not unfortunately obtained because of its poor stability caused by the strong electron-withdrawing property of CF_3. As shown in Fig. 4, Fe4 displays an *anti*-conformation. The calculated $\%V_{Bur}$ of Fe4 is 57.3, which is nearly the same as *anti*-Fe1 (57.2). Therefore, the substituent X mainly provides an electronic impact on iron complexes. Besides, crystal parameters in Table S1 (Supporting information) support that the presence of intramolecular π-π interactions in Fe4. The dihedral angle of Fe4 (12.43°) between the capping aryl group and the pyridyl ring is slightly larger than that of Fe1 (10.29°) while the centroid-centroid distance of Fe4 (3.24 Å) between the two aromatic rings is shorter than that of Fe1 (3.38 Å), indicating that the substituent X does not significantly change the π-π interaction. The π-π interaction regions (green regions) in Fe4 are graphically shown in Fig. 4.

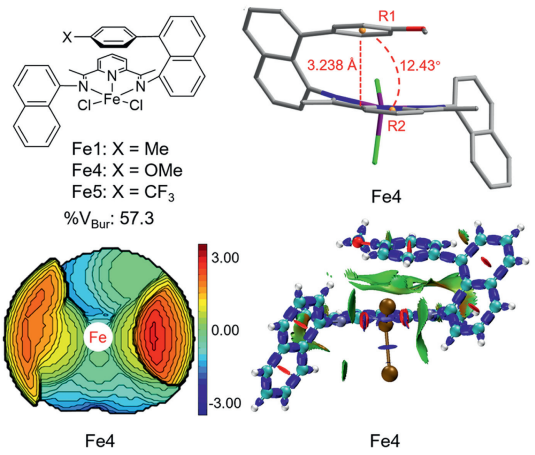

Fig. 4. Molecular structures, topographic steric map, and π-π interaction regions of bis(imino)pyridyl iron complexes.

Bis(imino)pyridyl iron complexes were used as catalyst precursors for ethylene polymerization after activation with 1000 equiv. MMAO at different polymerization temperatures. The effects of diastereomers, steric hindrance, weak π-π interaction, and electronic tuning on ethylene polymerization were extensively studied. It is previously reported that *syn*- and *anti*-diastereomers of α-diimine nickel and palladium catalysts often produce polyethylenes with markedly different molecular weight [42,45]. Although bis(imino)pyridyl iron complexes with different *ortho*-substituents on the aniline have been reported, *syn*- and *anti*-diastereomers are not considered due to the complex system [13–15,24–26]. Herein, single crystals of two diastereomers, *syn*-Fe1 and *anti*-Fe1, were chosen for ethylene polymerization to elucidate diastereomer effects of the iron complex.

Ethylene polymerization results (Table S5 in Supporting information) clearly show that *syn*-Fe1 and *anti*-Fe1 exhibit nearly the same ethylene polymerization behavior. Both *syn*-Fe1 and *anti*-Fe1 afford polyethylenes with nearly the same molecular weight and distribution, which is ascribed to dominant steric hindrance of capping aryl substituent and more open bis(imino)pyridyl chelating ring (N–N distance: bis(imino)pyridyl (4.21 Å) > α-diimine (2.45 Å)) [46]. The bimodal distribution of polyethylenes produced by Fe1 originates from two chain transfer pathways, including β-H transfer to ethylene monomer and chain transfer to aluminum co-catalyst [1,3]. Therefore, we do not consider the effects of *syn*- and *anti*-diastereomers of iron complexes on ethylene polymerization.

Four bis(imino)pyridyl iron complexes Fe0-Fe3 were used to study steric effects on ethylene polymerization. As shown in Table 1, the construction approach of bis(imino)pyridyl iron catalysts using two different anilines is highly effective based on steric tuning. The "sandwich" iron catalyst Fe3 is inactive in the temperature range of 30–90 °C for ethylene polymerization because of bulky hindrance, which is consistent with previous report [40]. However, the "half-sandwich" iron catalyst Fe1 with a capping aryl substituent is highly active (44.6×10^6 g_{PE} mol_{Fe}^{-1} h^{-1}). In comparison with Fe0 without capping aryl substituents, "half-sandwich" iron catalyst Fe1 is more thermally robust and produces higher molecular-weight polyethylenes (entry 4 *vs.* 8). Fe1 shows high activity of 10.4×10^6 g_{PE} mol_{Fe}^{-1} h^{-1} (entry 8) while Fe0 is inactive at 90 °C (entry 4) because of decomposition, indicating Fe1 has higher thermostability than Fe0.

The introduction of the methyl on the naphthyl group of Fe1 can further improve the thermostability of "half-sandwich" iron complex and PE molecular weight. The resultant iron catalyst Fe2 exhibits higher activity at high temperatures (≥90 °C) than Fe1 although Fe2 is less active at low temperatures (≤70 °C). Iron complex Fe2 is still active to produce narrowly dispersed PE at an elevated temperature of 130 °C while Fe1 is inactive for ethylene polymerization, supporting that Fe2 is more thermally stable than Fe1. To the best of our knowledge, the elevated temperature of 130 °C represents the highest temperature of ethylene polymerization using bis(imino)pyridyl iron catalysts [13,26]. The enhanced thermostability of "half-sandwich" iron catalysts Fe1 and Fe2 is reasonably ascribed to the intramolecular π-π interaction between the capping aryl substituent and the pyridyl ring. The intramolec-

Table 1
Ethylene polymerization results using bis(imino)pyridyl iron catalysts.[a]

Entry	Fe	T (°C)	Yield (g)	Activity ($\times 10^6$ g_{PE} mol_{Fe}^{-1} h^{-1})	M_n (kg/mol)[b]	M_w (kg/mol)[b]	$Đ$[b]	T_m (°C)[c]
1	Fe0	30	5.08	25.4	1.2	5.4	4.5	117.8
2	Fe0	50	6.17	30.8	1.4	9.6	6.9	119.1
3	Fe0	70	3.74	18.7	2.9	13.2	4.6	120.1
4	Fe0	90	-	-	-	-	-	-
5	Fe1	30	2.57	12.9	1.7	15.4	9.1	122.1
6	Fe1	50	5.89	29.5	2.3	28.6	12.4	124.4
7	Fe1	70	8.92	44.6	2.8	31.6	11.3	125.5
8	Fe1	90	2.07	10.4	1.7	22.0	12.9	123.4
9	Fe1	110	-	-	-	-	-	-
10	Fe2	30	2.43	12.2	2.3	27.5	12.0	127.0
11	Fe2	50	4.77	23.9	2.9	29.7	10.2	127.2
12	Fe2	70	7.12	35.6	3.4	32.4	9.5	126.4
13	Fe2	90	4.59	22.9	2.5	30.4	12.2	126.1
14	Fe2	110	1.88	9.4	1.6	25.2	15.8	125.5
15	Fe2	130	0.78[d]	3.9	1.0	2.5	2.5	118.6
16	Fe3	30∼90	-	-	-	-	-	-

-: No activity and not determined.
[a] Polymerization conditions: 2.4 μmol iron catalyst, Al(MMAO)/Fe = 1000, 10 atm ethylene pressure, 5 min, 68 mL of toluene and 2 mL of CH_2Cl_2.
[b] Determined by GPC in 1,2,4-trichlorobenzene at 150 °C.
[c] Determined by DSC, second heating.
[d] Solid product is isolated and is used to calculate activity.

Table 2
Ethylene polymerization results using bis(imino)pyridyl iron catalysts.[a]

Entry	Fe	X	T (°C)	Yield (g)	Activity ($\times 10^6$ g_{PE} mol_{Fe}^{-1} h^{-1})	M_n (kg/mol)[b]	M_w (kg/mol)[b]	$Đ$[b]	T_m (°C)[c]
1	Fe4	OMe	30	3.93	19.7	2.2	13.5	6.1	120.8
2	Fe4	OMe	50	6.13	30.7	2.2	24.7	11.2	124.0
3	Fe4	OMe	70	5.02	25.1	2.1	19.4	9.2	123.8
4	Fe4	OMe	90	1.96	9.8	2.1	16.0	7.6	122.6
5	Fe5	CF_3	30	1.00	5.0	2.9	37.1	12.8	126.1
6	Fe5	CF_3	50	4.63	23.2	3.8	87.5	23.0	128.6
7	Fe5	CF_3	70	2.47	12.4	2.7	35.0	13.0	125.8
8	Fe5	CF_3	90	0.31	1.6	1.1	1.6	1.5	124.4

[a] Polymerization conditions: 2.4 μmol iron catalyst, Al(MMAO)/Fe = 1000, 10 atm ethylene pressure, 5 min, 68 mL of toluene and 2 mL of CH_2Cl_2.
[b] Determined by GPC in 1,2,4-trichlorobenzene at 150 °C.
[c] Determined by DSC, second heating.

ular π-π interaction is anticipated to restrict the *N*-aryl rotation and fix the capping aryl substituent above the chelating ring at elevated temperatures, thereby enhancing the thermal stability of iron complexes [33,46]. Besides, narrow distribution of PEs produced by less bulky Fe0 is ascribed to small molecular weight difference through β-H transfer to monomer and chain transfer to aluminum cocatalyst. However, narrow distribution of the PE produced by Fe2 at 130 °C should be a result of chain transfer to aluminum (see below discussion on the effect of temperature on chain transfer).

The electronic effects were further evaluated by ethylene polymerizations catalyzed by three iron catalysts with different X substituents (X = Me, OMe, CF_3). It is known that the electronic effects of substituent X on the phenyl group can be quantitatively reflected by Hammett constants (σ) [47]. The electron-donating ability of substituent X decreases in the order of OMe (σ: −0.268) > Me (σ: −0.170) > CF_3 (σ: +0.540) based on σ values. Ethylene polymerization results of iron catalysts Fe4 and Fe5 are listed in Table 2, and the comparisons of ethylene polymerization results using three catalysts Fe1, Fe4, and Fe5 are directly revealed in Fig. S13 (Supporting information).

As shown in Fig. S13, Fe1 shows the highest activity among three iron catalysts while electron-deficient Fe5 with CF_3 produces the highest molecular weight PE. This observation is reasonably explained by electronic effects of the substituent X [48,49]. Naturally, the electronic effects on ethylene polymerization are reflected in the electrophilicity of the metal center and catalyst stability. Usually, the introduction of the electron-withdrawing CF_3 group increases the electrophilicity of the metal center, which increases the rate of ethylene coordination and insertion. Resultantly, enhanced chain growth rate leads to high-molecular-weight PE. On the other hand, the introduction of electron-withdrawing groups often leads to poor stability, which causes low initiator efficiency and catalyst lifetime. In fact, iron complex Fe5 has the poorest stability in solution (see detail complex synthesis in Supporting information). Resultantly, electron-deficient Fe5 with CF_3 shows the lowest activity but affords higher-molecular weight PE. On the contrary, the introduction of electron-donating OMe group slows down the chain growth rate but accelerates the chain transfer rate. Therefore electron-rich Fe4 with OMe produces the lowest-molecular-weight PE.

It is worth noting that bimodal distribution polyethylenes were produced by bis(imino)pyridyl iron catalysts, which is a result of two chain transfer pathways including β-H transfer to monomer and chain transfer to aluminum cocatalyst [1,3,50]. Herein, Fe5 was chosen to conduct mechanistic study of chain transfer. Firstly, the effect of Al/Fe mole ratio on chain transfer was examined (Table S6 in Supporting information). As shown in Fig. 5, GPC curves of PEs are bimodal distribution, and are reasonably divided into two components with normal distributions (Fig. S20 in Supporting information). At low Al/Fe ratio of 500, the high-molecular-weight fraction is dominant and a small tail peak is attributed to the low-molecular-weight fraction, indicating that β-H transfer to ethylene is the main chain transfer pathway at a low Al/Fe ratio. With increasing Al/Fe ratio from 500 to 2000, the proportion of low-

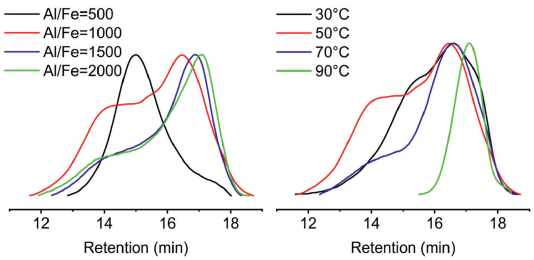

Fig. 5. GPC curves of the PEs produced by Fe5 at different Al/Fe ratios (left) and temperatures (right).

molecular-weight fraction increases and shifts to lower-molecular-weight region, further proving that low-molecular-weight fraction is subject to chain transfer to aluminum and high-molecular-weight fraction is subject to β-H transfer to ethylene.

The effect of temperature on chain transfer was further studied. GPC curves of PEs produced at different temperatures (Fig. 5) clearly show that the proportion of high-molecular-weight fraction decreases with an increase in polymerization temperature from 30 °C to 90 °C. However, the GPC curve of PE is monomodal distribution at 90 °C, indicating only one chain transfer pathway. ^{1}H and ^{13}C NMR analysis of chain-end groups of PEs produced at 90 °C clearly confirm that the obtained PE at 90 °C is fully saturated and linear polyethylene without a vinyl end (Figs. S16-S19 in Supporting information). This result strongly proves that chain transfer to aluminum only takes place at a high temperature of 90 °C for Fe5. Besides, ethylene polymerization results at different ethylene pressures show that PE molecular weight increases with increasing ethylene pressure, further indicating occurrence of chain transfer to aluminum (Table S7 in Supporting information). From these results, it is safely concluded that chain transfer to aluminum more easily take place than β-H transfer to ethylene at elevated temperatures for Fe5. However, distributions of PEs produced by Fe1 are not big change at 30–90 °C due to the appearance of two chain transfer pathways. This difference of the temperature effect on distribution should be a result of the electronic effect. Our study initially clarifies the effect of polymerization temperature on chain transfer and provides access to the synthesis of monomodal and saturated polyethylene wax using bis(imino)pyridyl iron catalysts at high temperatures.

In summary, we have successfully designed and synthesized a series of "half-sandwich" bis(imino)pyridyl iron complexes with a substituted 8-(*p*-X-phenyl)naphthylamine (X = OMe, Me, CF_3) by combining weak π-π interaction with steric and electronic tunings. Ethylene polymerization results clearly illuminate the roles of weak π-π interaction, steric bulk, and electronic tuning. The synergy combination of π-π interaction with steric and electronic tunings can access to the most thermally stable bis(imino)pyridyl iron catalyst up to 130 °C. Bimodal distribution of resultant PEs originates from two chain transfer pathways involving β-H transfer to ethylene and chain transfer to aluminum, and the chain transfer pathway can be regulated by Al/Fe mole ratio and temperature.

Declaration of competing interest

The authors declare that they have no known competing financial interests or personal relationships that could have appeared to influence the work reported in this paper.

CRediT authorship contribution statement

Heng Gao: Writing – original draft, Formal analysis, Data curation, Conceptualization. **Zhaocong Cheng:** Methodology, Formal analysis, Data curation. **Guangshui Tu:** Formal analysis, Data curation. **Zonglin Qiu:** Software, Formal analysis. **Xieyi Xiao:** Resources, Data curation. **Haotian Zhou:** Formal analysis, Data curation. **Handou Zheng:** Writing – review & editing, Investigation, Funding acquisition. **Haiyang Gao:** Writing – review & editing, Supervision, Project administration.

Acknowledgments

This work was financially supported by the State Key Research Development Program of China (No. 2021YFB3800701), National Natural Science Foundation of China (NSFC, No. 52173016), Guangdong Basic and Applied Basic Research Foundation (Nos. 2024A1515012784, 2024A1515011102, and 2023A1515110549), Fundamental Research Funds for the Central Universities, Sun Yat-sen University (No. 24qnpy047), and PetroChina Scientific and Technological Projects (No. 2022DJ6308).

Supplementary materials

Supplementary material associated with this article can be found, in the online version, at doi:10.1016/j.cclet.2024.110762.

References

[1] B.L. Small, M. Brookhart, A.M.A. Bennett, J. Am. Chem. Soc. 120 (1998) 4049–4050.
[2] G.J.P. Britovsek, V.C. Gibson, B.S. Kimberley, et al., Chem. Commun. 7 (1998) 849–850.
[3] G.J.P. Britovsek, M. Bruce, V.C. Gibson, et al., J. Am. Chem. Soc. 121 (1999) 8728–8740.
[4] V.C. Gibson, C. Redshaw, G.A. Solan, Chem. Rev. 107 (2007) 1745–1776.
[5] Z. Flisak, W.H. Sun, ACS Catal. 5 (2015) 4713–4724.
[6] B.L. Small, Acc. Chem. Res. 48 (2015) 2599–2611.
[7] T. Liu, Y.P. Ma, G.A. Solan, Y. Sun, W.H. Sun, New J. Chem. 47 (2023) 5786–5795.
[8] C. Bariashir, Z. Wang, Y.P. Ma, et al., Organometallics 38 (2019) 4455–4470.
[9] C. Bianchini, G. Mantovani, A. Meli, et al., Eur. J. Inorg. Chem. 2003 (2003) 1620–1631.
[10] L. Zhong, H.D. Zheng, C. Du, et al., J. Catal. 384 (2020) 208–217.
[11] H.D. Zheng, Z.L. Qiu, H. Gao, et al., Macromolecules 57 (2024) 5279–5288.
[12] Q. Wang, Z. Zhang, C. Zou, C.L. Chen, Chin. Chem. Lett. 33 (2022) 4363–4366.
[13] Q. Mahmood, J.J. Guo, W.J. Zhang, et al., Organometallics 37 (2018) 957–970.
[14] L.W. Guo, W.J. Zhang, F.R. Cao, et al., Polym. Chem. 12 (2021) 4214–4225.
[15] L.H. Guo, H.Y. Gao, L. Zhang, F.M. Zhu, Q. Wu, Organometallics 29 (2010) 2118–2125.
[16] J. Ma, C. Feng, S.L. Wang, et al., Inorg. Chem. Front. 1 (2014) 14–34.
[17] W.J. Zhang, W.H. Sun, C. Redshaw, Dalton Trans. 42 (2013) 8988–8997.
[18] W.H. Sun, W.Z. Zhao, J.G. Yu, Macromol. Chem. Phys. 213 (2012) 1266–1273.
[19] Z. Wang, G.A. Solan, W.J. Zhang, W.H. Sun, Coord. Chem. Rev. 363 (2018) 92–108.
[20] R.D. Zhang, M.Y. Han, Y.P. Ma, et al., Dalton Trans. 48 (2019) 17488–17498.
[21] J.G. Yu, H. Liu, W.J. Zhang, X. Hao, W.H. Sun, Chem. Commun. 47 (2011) 3257–3259.
[22] N.E. Mitchell, W.C. Anderson Jr., B.K. Long, J. Polym. Sci., Part A: Polym. Chem. 55 (2017) 3990–3995.
[23] Y.X. Zhang, C.Q. Wang, Z.B. Jian, Eur. Polym. J. 128 (2020) 109605.
[24] X.P. Cao, F. He, W.Z. Zhao, et al., Polymer 53 (2012) 1870–1880.
[25] S.L. Wang, B.X. Li, T.L. Liang, et al., Dalton Trans. 42 (2013) 9188–9197.
[26] K.F. Tahir, Y.P. Ma, Q. Mahmood, et al., Polymer 308 (2024) 127335.
[27] H.D. Zheng, H.Y. Gao, Macromolecules 57 (2024) 6899–6913.
[28] K.T. Mahmudov, A.V. Gurbanov, F.I. Guseinov, M.F. Guedes Da Silva, Coord. Chem. Rev. 387 (2019) 32–46.
[29] C.L. Chen, Nat. Rev. Chem. 2 (2018) 6–14.
[30] L. Falivene, L. Cavallo, G. Talarico, Mol. Catal. 494 (2020) 111118.
[31] X.H. Wang, B. Dong, Q. Yang, et al., Polym. Chem. 11 (2020) 6783–6793.
[32] T. Vaidya, K. Klimovica, A.M. LaPointe, et al., J. Am. Chem. Soc. 136 (2014) 7213–7216.
[33] Y.F. Gong, S.K. Li, C. Tan, et al., J. Catal. 378 (2019) 184–191.
[34] Z.F. Xiao, H.D. Zheng, C. Du, et al., Macromolecules 51 (2018) 9110–9121.
[35] B.B. Wang, H. Liu, C.Y. Zhang, T. Tan, X.Q. Zhang, Polym. Chem. 12 (2021) 6307–6318.
[36] F. Lin, M. Voccia, L. Odenwald, et al., J. Am. Chem. Soc. 145 (2023) 27950–27957.
[37] L. Falivene, T. Wiedemann, I. Göttker–Schnetmann, et al., J. Am. Chem. Soc. 140 (2018) 1305–1312.
[38] M. Li, X.B. Wang, Y. Luo, C.L. Chen, Angew. Chem. Int. Ed. 56 (2017) 11604–11609.
[39] C.S. Popeney, A.L. Rheingold, Z.B. Guan, Organometallics 28 (2009) 4452–4463.
[40] Z.C. Cheng, H. Gao, Z.L. Qiu, et al., ACS Catal. 14 (2024) 7956–7966.

[41] L.Y. Wang, W.H. Sun, L.Q. Han, et al., J. Organomet. Chem. 658 (2002) 62–70.
[42] B. Wang, O. Daugulis, M. Brookhart, Organometallics 38 (2019) 4658–4668.
[43] L. Falivene, Z. Cao, A. Petta, et al., Nat. Chem. 11 (2019) 872–879.
[44] T. Lu, Q.X. Chen, Chemistry–Methods 1 (2021) 231–239.
[45] H.Y. Gao, F.S. Liu, H.B. Hu, F.M. Zhu, Q. Wu, Chin. J. Polym. Sci. 31 (2013) 563–573.
[46] H.D. Zheng, Y.W. Li, W.B. Du, et al., Macromolecules 55 (2022) 3533–3540.
[47] L.P. Hammett, J. Am. Chem. Soc. 59 (1937) 96–103.
[48] H.D. Zheng, L.X. Pei, H.Y. Deng, H. Gao, H.Y. Gao, Eur. Polym. J. 184 (2023) 111773.
[49] H.L. He, W.B. Wang, W.M. Pang, C. Zou, D. Peng, Chin. Chem. Lett. 35 (2024) 109534.
[50] N.V. Semikolenova, W.H. Sun, I.E. Soshnikov, et al., ACS Catal. 7 (2017) 2868–2877.